The Journal of Chemical Physics

A spectroscopic model for the low-lying electronic states of NO

Cite as: J. Chem. Phys. **154**, 074112 (2021); https://doi.org/10.1063/5.0038527
Submitted: 24 November 2020 . Accepted: 15 January 2021 . Published Online: 19 February 2021

Qianwei Qu, Bridgette Cooper, Sergei N. Yurchenko, and Jonathan Tennyson

COLLECTIONS

Paper published as part of the special topic on Quantum Dynamics with ab Initio Potentials

The Journal of Chemical Physics ARTICLE scitation.org/journal/jcp

A spectroscopic model for the low-lying electronic states of NO

Cite as: J. Chem. Phys. 154, 074112 (2021); doi: 10.1063/5.0038527
Submitted: 24 November 2020 • Accepted: 15 January 2021 •
Published Online: 19 February 2021

Qianwei Qu, Bridgette Cooper, Sergei N. Yurchenko, and Jonathan Tennyson[a)]

AFFILIATIONS

Department of Physics and Astronomy, University College London, London WC1E 6BT, United Kingdom

Note: This paper is part of the JCP Special Topic on Quantum Dynamics with *Ab Initio* Potentials.
[a)]**Author to whom correspondence should be addressed:** j.tennyson@ucl.ac.uk

ABSTRACT

The rovibronic structure of $A^2\Sigma^+$, $B^2\Pi$, and $C^2\Pi$ states of nitric oxide (NO) is studied with the aim of producing comprehensive line lists for its near ultraviolet spectrum. Empirical energy levels for the three electronic states are determined using a combination of the empirical measured active rotation–vibration energy level (MARVEL) procedure and *ab initio* calculations, and the available experimental data are critically evaluated. *Ab initio* methods that deal simultaneously with the Rydberg-like $A^2\Sigma^+$ and $C^2\Pi$ and the valence $B^2\Pi$ state are tested. Methods of modeling the sharp avoided crossing between the $B^2\Pi$ and $C^2\Pi$ states are tested. A rovibronic Hamiltonian matrix is constructed using the variational nuclear motion program Duo whose eigenvalues are fitted to the MARVEL. The matrix also includes coupling terms obtained from the refinement of the *ab initio* potential energy and spin–orbit coupling curves. Calculated and observed energy levels agree well with each other, validating the applicability of our method and providing a useful model for this open shell system.

I. INTRODUCTION

Nitric oxide (NO) is one of the principle oxides of nitrogen. It plays a significant role in the nitrogen cycle of our atmosphere[1,2] but also causes problems of air pollution and acid rain.[3–5] Therefore, scientists are devoting increasing attention to reducing NO in combustion processes.[6,7] NO is a biological messenger for both animals and plants,[8–10] but it may be harmful or even deadly as well.[11,12] Apart from on Earth, NO was also observed in the interstellar environments and atmospheres of other planets.[13–16]

The importance of NO has aroused the interest of academia and industry since it was prepared by van Helmont in the 17th century[17] and then studied by Priestley in 1772.[18] In numerous theoretical and experimental works, there are a large number of spectroscopic investigations, as spectra provide a powerful weapon to reveal the physical and chemical properties of the molecule. For instance, as a stable open shell molecule, the electronically excited Rydberg states of NO have been extensively studies (see the paper of Deller and Hogan[19] and references therein). The spectrum of NO was also of great value in many applications, such as temperature measurements by laser induced fluorescence.[20,21]

The ExoMol project[22] computes molecular line list studies of exoplanet and (other) hot atmospheres. The ExoMol database was formally released in 2016.[23] The most recent 2020 version[24] covers the line lists of 80 molecules and 190 isotopologues, totaling 700×10^9 transitions. It includes an accurate infrared (IR) line list of NO, called `NOname`, which contains the rovibrational transitions within the ground electronic state.[25] The rovibronic transitions of NO in the ultraviolet (UV) region are not included in `NOname`. These bands are strong and atmospherically important and have been observed in many studies.[26–28] There is no NO UV line list in well-known databases such as HITRAN (high transmission molecular absorption)[29] and GEISA (Gestion et Etude des Informations Spectroscopiques Atmosphériques).[30]

Luque and Crosley investigated the spectra of diatomic molecules over a long period.[31–33] Based on their works, they developed a spectral simulation program, LIFBASE,[34] providing a database of OH, OD, CH, etc., and NO as well. LIFBASE contains the positions and relative probabilities of UV transitions in four spectral systems of NO, i.e., γ ($A^2\Sigma^+$ to $X^2\Pi$), β ($B^2\Pi$ to $X^2\Pi$), δ ($C^2\Pi$ to $X^2\Pi$), and ϵ ($D^2\Sigma^+$ to $X^2\Pi$) systems. The upper vibrational energy

levels for $B^2\Pi$ and $C^2\Pi$ of NO in LIFBASE are limited to below $v = 7$ and $v = 1$, respectively. However, the observed β and δ transitions corresponding to higher upper vibrational energy levels are even stronger.[28,35] There is a need to develop a comprehensive UV line list for NO to cover these band systems. To do this, one first needs to construct a spectroscopic model that requires overcoming a number of theoretical difficulties. The purpose of this paper is to present our model and explain how we resolve these difficulties.

A major issue in generating a UV line list for NO results from the difficulty of modeling the interaction between $B^2\Pi$ and $C^2\Pi$ states, which is caused by the particular electronic structure of NO. To understand this 15 electron system, one must analyze the electron configuration of these states from the perspective of molecular orbitals. On the one hand, excitation of inner paired electrons to higher valence orbitals leads to valence states such as $B^2\Pi$. On the other hand, the outermost unpaired electron may be excited to Rydberg orbitals, yielding a series of Rydberg states such as $A^2\Sigma^+$ or $C^2\Pi$. These Rydberg states lie close in energy to the valence ones. Furthermore, as NO^+ has a shorter equilibrium bond length than NO,[36] Rydberg states tend to be lower in energy at short bond lengths, r, while valence states are lower at larger r. Thus, in NO, Rydberg–valence interactions are densely distributed in the neighborhood of the equilibrium bond length of its ground state, where large Franck–Condon factors exist. The $B^2\Pi$–$C^2\Pi$ interaction is the lowest one and has attracted the most attention. As described by Lagerqivst and Miescher,[26] the two states show a strong and extended mutual perturbation. They proposed a "deperturbation" method to explain the vibrational and rotational perturbation of $B^2\Pi$–$C^2\Pi$ interaction. Further analysis was made by Gallusser and Dressler,[37] who set up a vibronic interaction matrix of five $^2\Pi$ states and fitted the eigenvalues of the matrix to experimental data in the determination of Rydberg–Klein–Rees (RKR) potential curves and off-diagonal electronic energies. As a consequence, they predicted vibrational states of the $B^2\Pi$ electronic state up to $v = 37$.

In this paper, we propose a method based on directly diagonalizing a rovibronic matrix to resolve the energy structures of $B^2\Pi$–$C^2\Pi$ coupled states. This matrix is based on the use of full variational solution of the rovibronic nuclear motion Hamiltonian rather than perturbation theory. This method is general and can be used to predict spectra, for example, at elevated temperatures.

In addition to the vibronic matrix elements (e.g., spin doublets) considered in the previous studies, more fine structure terms, such as Λ − *doubling* and spin–rotational coupling, are used to construct the rovibronic matrix. The eigenvalues of the matrix are fitted to rovibronic energies obtained using a MARVEL (measured active rotation-vibration energy level) procedure[38,39] analysis of the observed NO IR/visible/UV transitions to ensure a quantitatively accurate result. Figure 1 summarizes the band systems involved in our MARVEL analysis. The objective functions were constrained with the *ab initio* curves produced using Molpro[40] to avoid overfitting problems. The above procedures are also applied to the $A^2\Sigma^+$ state of NO to get a self-consistent description of the doublet electronic states up to and including $C^2\Pi$.

This work forms the foundation of our future study on the generation of the UV line list of NO. The modeling of $B^2\Pi$–$C^2\Pi$ paves the way for the investigations of molecules with similar avoided crossing structures.

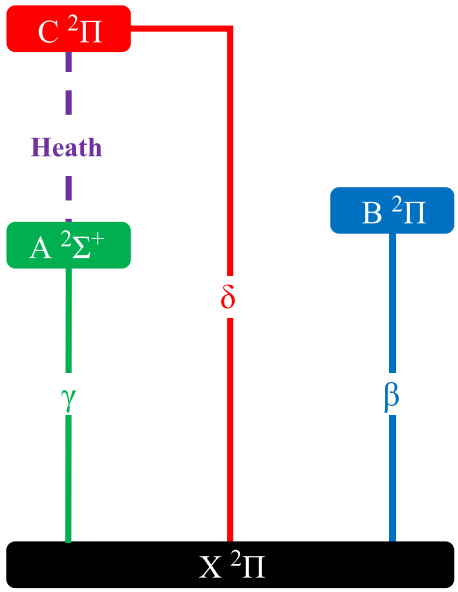

FIG. 1. The band systems of NO involved in this work and their names. The γ, β, and δ systems mainly cover the UV transitions of NO. Jenkins *et al.* recorded many visible lines from the $B^2\Pi$ state to higher vibrational levels of $X^2\Pi$, e.g., those of the β(3, 16) band.[41] The high-accuracy IR transitions of the Heath (0, 0) band were measured by Amiot and Verges.[42] For a comprehensive band system diagram, see the work of Cartwright *et al.*[43]

II. THEORETICAL STUDY OF THE LOW-LYING ELECTRONIC STATES OF NO

Complete active space self-consistent field (CASSCF) and multireference configuration interaction (MRCI) calculations were performed in the quantum chemistry package Molpro 2015[44] to get the potential energy and spin–orbit curves of the $X^2\Pi$, $A^2\Sigma^+$, $B^2\Pi$, and $C^2\Pi$ states. A major issue in the calculation is achieving a balance between representations of the Rydberg, A and C, states and the valence, X and B, states. Figure 2 presents an overview of the low-lying potential energy curve (PECs) and illustrates the importance of the $C^2\Pi$–$B^2\Pi$ Rydberg–valence avoided crossing.

The history of high quality configuration interaction (CI) calculation for the excited states of NO can be tracked back to 1982, when Grein and Kapur reported their work on the states with the minimum electronic energies lower than 6.58 eV.[45] Several years later, a comprehensive theoretical study on NO was presented and discussed by de Vivie and Peyerimhoff.[46] The results of this paper were further improved by Shi and East in 2006.[47] More accurate curves were obtained with extended basis set and active space in the recent works of Cheng *et al.*[48,49] Although the previous works[45–48,50–53] provide us strong inspiration, the task is still challenging due to the interactions between Rydberg and valence states of NO.

A. Active space and basis set

For heteronuclear diatomic molecules, Molpro executes calculations in four irreducible representations a_1, b_1, b_2, and a_2 of the C_{2v}

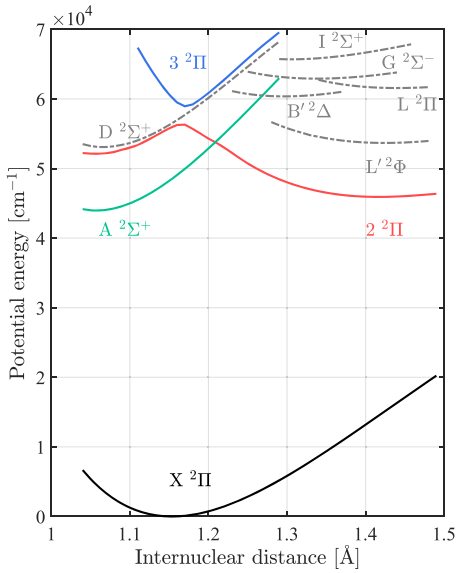

FIG. 2. NO PECs calculated by Shi and East.[47] The states of interest are plotted by solid curves. Here, $2^2\Pi$ is the $B^2\Pi$ to $C^2\Pi$ PEC, while $3^2\Pi$ is the $C^2\Pi$ to $B^2\Pi$ PEC.

point group. Here, we use $[(n_1, n_2, n_3, n_4) - (n_1', n_2', n_3', n_4')]$ to represent occupied orbitals excluding closed orbitals, i.e., the calculation active space. A typical active space for the lower electronic states calculation of NO is $[(8, 3, 3, 0) - (2, 0, 0, 0)]$, as suggested by Shi and East.[47] Although only a few of the PECs are of direct interest here, we had to include extra states to achieve correct calculation. We also adjusted the active space to get smooth curves.

A Dunning aug-cc-pV(n)Z basis set[54] was used in both CASSCF and MRCI calculations. This basis set has an additional shell of diffuse functions compared to the cc-pV(n)Z basis set, which benefits the calculation of Rydberg states. Too many diffuse functions, e.g., those of the d-aug-cc-pV(n)Z basis set, may have negative effects on the calculation because of the overemphasis of the Rydberg states relative to the valence states.

B. CASSCF calculation

Our calculations started with a $[(8, 3, 3, 0) - (2, 0, 0, 0)]$ active space in which the interactions between the Rydberg and valence states are inescapable. However, representing the avoided crossing points caused by $C^2\Pi$ and the valence $^2\Pi$ states proved to be a huge obstacle to obtaining satisfactory results. Panel (a) of Fig. 3 shows the terrible behavior of B–C interaction near 1.18 Å. The potential energy curve (PEC) of $C^2\Pi$ suddenly jumps to that of $B^2\Pi$, producing discontinuity in the PEC of $X^2\Pi$ too. To get the exited states, we used the state average algorithm, but the average energy of the two $^2\Pi$ states changed when traversing the crossing point of $C^2\Pi$ and $B^2\Pi$.

A valid way to smooth the curves is to increase the number of averaged states. For example, the discontinuities near 1.18 Å disappear when introducing a third $^2\Pi$ state in CASSCF calculation, as shown in panel (b) of Fig. 3. Nevertheless, similar phenomenon arises when the third state comes across $L^2\Pi$. Alternatively, smooth curves can be obtained in limited active space. For example, we can get a continuous curves of $C^2\Pi$ in the active space $[(6, 3, 3, 0) - (4, 1, 1, 0)]$ from 0.9 Å to 1.28 Å.

We always started a new CASSCF iteration from the orbitals of a nearby geometry to stabilize and accelerate the calculation. The PECs in panels (a) and (b) of Fig. 3 are obtained by increasing the internuclear distance from 0.9 Å to 1.3 Å. Interestingly, with an

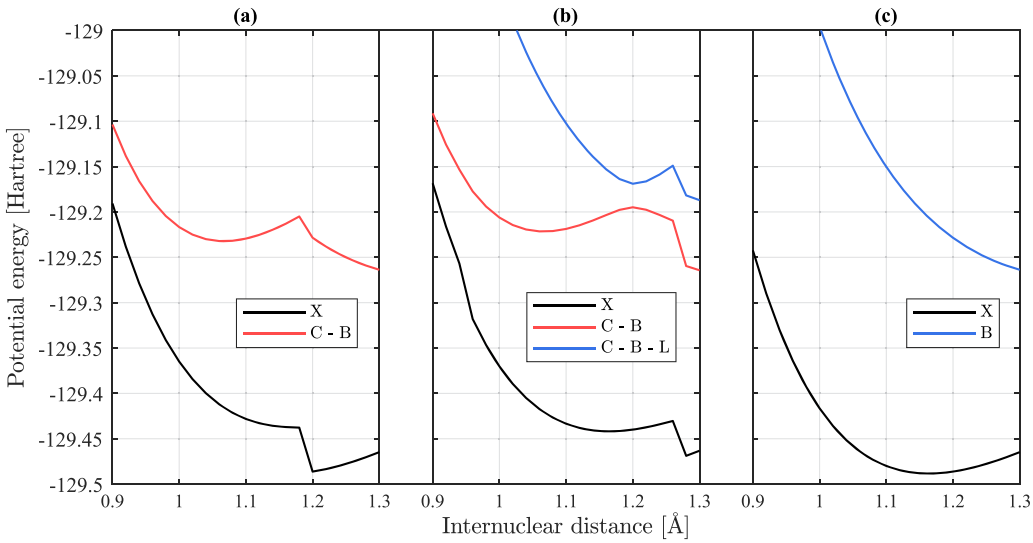

FIG. 3. The PECs in the active space of $[(8, 3, 3, 0) - (2, 0, 0, 0)]$ with the basis set of aug-cc-pVTZ. (a) Two $^2\Pi$ state averaged CASSCF calculation starting from 0.9 Å. (b) Three $^2\Pi$ state averaged CASSCF calculation starting from 0.9 Å. (c) Two $^2\Pi$ states averaged CASSCF calculation starting from 1.3 Å.

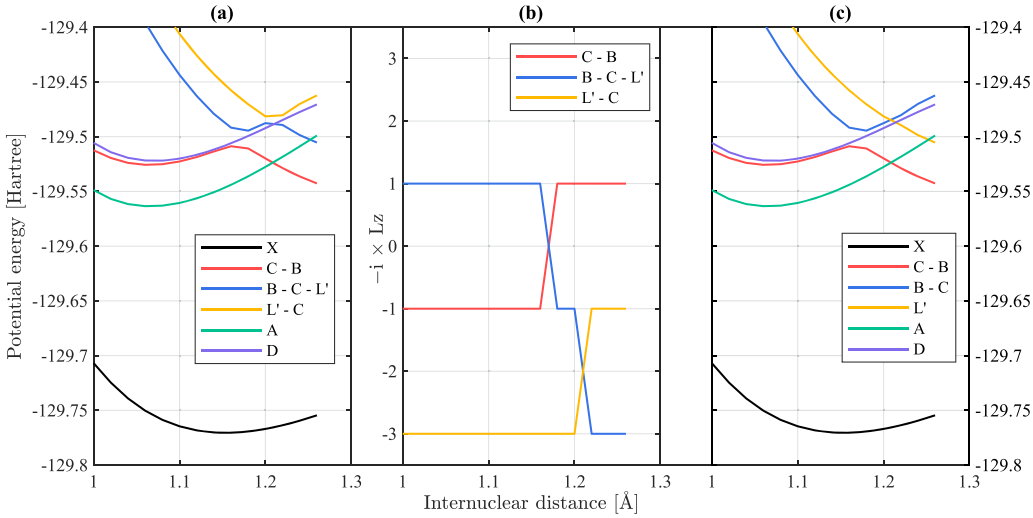

FIG. 4. The PECs of the $X^2\Pi$, $A^2\Sigma^+$, $B^2\Pi$, $C^2\Pi$, $D^2\Sigma^+$, and $L'^2\Phi$ states, obtained by CASSCF and MRCI + Q calculation starting from 1.06 Å to both sides in the active space [(8, 3, 3, 0) − (2, 0, 0, 0)] with the aug-cc-pV5Z basis set. The third $^2\Pi$ curve and the $L'^2\Phi$ curve in panel (a) were manually switched in panel (c) on the right of 1.2 Å, according to the value of Lz, shown in panel (b). The phase of Lz, in the Cartesian representation, is random. To distinguish different electronic states, the yellow curve in panel (b) is smoothed for internuclear distances less than 1.1 Å. The $X^2\Pi$ state is not shown in the panel as the Lz values obtained are all −i.

initial geometry at 1.3 Å, reversing the calculation direction gives a completely different result in the same active space, i.e., two smooth valence PECs of $X^2\Pi$ and $B^2\Pi$ states in panel (c) of Fig. 3. Due to the limitation of nonlinear programming, CASSCF iterations may fall into local minima. To get the target states, the numerical optimization must be properly initialized. For the NO molecule, the iterations that begin with valence orbitals usually end with valence orbitals, but it is uncertain for those beginning with Rydberg orbitals. The results imply that there are at least two kinds of local minima in the *ab initio* calculation of NO with Molpro: pure valence orbitals [corresponding to panel (c) of Fig. 3] and Rydberg-valence hybrid orbitals [corresponding to panels (a) and (b) of Fig. 3]. To verify the conjecture: initializing a calculation of two $^2\Pi$ states average with the CASSCF orbitals of the $X^2\Pi$ state in the single state calculation, one can get almost the same curves as those in panel (c) of Fig. 3, starting from 0.9 Å.

In Sec. IV, we use diabatic potentials in modeling the interaction between $B^2\Pi$ and $C^2\Pi$ states. We describe the curves as "adiabatic" if they contain the B–C avoided crossing feature, e.g., those in panel (b) of Fig. 3. If not, we call the curves "diabatic," e.g., those in panel (c) of Fig. 3.

C. MRCI calculation

Although consuming many more computational resources, the MRCI calculation in Molpro is straightforward. Molpro automatically takes the CASSCF orbitals as the references and performs an internally contracted configuration interaction calculation based on single or double excitation. The spin–orbit coupling (SOC) terms were also produced. To compensate the error brought by the truncated configuration interaction expansion, the energies were modified by Davision correction, i.e., MRCI + Q calculation. Panel (a) of Fig. 4 demonstrates the results of CASSCF and MRCI + Q calculation of the $X^2\Pi$, $A^2\Sigma^+$, $B^2\Pi$, $C^2\Pi$, $D^2\Sigma^+$, and $L'^2\Phi$ states, in [(8, 3, 3, 0) − (2, 0, 0, 0)] active space with the aug-cc-pV5Z basis set.

In the CASSCF routine, the projection of angular momentum of a diatomic molecule on its internuclear axis, Λ, can be assigned to specify the expected states. However, the MRCI routine does not have the option and always finds the lowest energy states of the same spin. As a result, the PECs of $C^2\Pi$ and $L'^2\Phi$ exchange with each other at their crossing point although the avoided crossing principle is not applicable for the two states, as shown by the blue curve in panel (a) of Fig. 4. It is feasible to calculate and output the Λ quantum numbers (technically, Lz, which is defined as a non-diagonal matrix element between two degenerate components, e.g., $\langle\Pi_x|\hat{L}_z|\Pi_y\rangle$) in MRCI calculations, which helps to distinguish the $C^2\Pi$, $L'^2\Phi$, and $L^2\Pi$ states. The blue and yellow curves on the right of their crossing point were manually switched, as shown in panel (c) of Fig. 4, according to their Λ quantum numbers shown in panel (b). The T_e values of $A^2\Sigma^+$, $B^2\Pi$, and $C^2\Pi$ states are compared with those calculated by Shi and East in Table I.

TABLE I. Comparison of T_e values of the MRCI + Q calculation.

	CASSCF and MRCI + Q		Empirical	
State	Shi and east[47]	This work	Huber and herzberg[55]	This work[a]
$A^2\Sigma^+$	43 558	45 410.2	43 965.7	43 902.99
$B^2\Pi$	44 803	46 260.3[b]	45 913.6	45 867.05
$C^2\Pi$	51 808	53 709.5	52 126	52 081.97

[a]See Sec. IV.
[b]Two-state average CASSCF and MRCI + Q calculation.

The PECs in Fig. 4 range from 1.0 Å–1.26 Å. The curves were deliberately truncated at the right endpoint because of the $C^2\Pi$–$L^2\Pi$ interaction, as shown in panel (b) of Fig. 3. On the left endpoint, the MRCI program exited with an "INSUFFICIENT OVERLAP" error. The error is triggered by interactions with another $^2\Pi$ state, $H'^2\Pi$, which lies below $B^2\Pi$ near the 1.06 Å and which cannot be described by the reference space. A solution to the problem is to perform MRCI calculations using a larger active space such as [(8, 4, 4, 0) − (2, 0, 0, 0)].

It is not quantitatively accurate to generate line lists with the *ab initio* curves; however, the curves and couplings provide a suitable starting point for work. These curves and couplings need to be refined using experimental data, which is the content of Secs. III and IV.

III. MARVEL ANALYSIS OF THE ROVIBRONIC ENERGY LEVELS OF $^{14}N^{16}O$

The rovibronic energy levels of $A^2\Sigma^+$, $B^2\Pi$, and $C^2\Pi$ states were reconstructed by MARVEL analysis of the experimental transitions of the γ, β, δ, and Heath systems and those inside the ground state.

In the previous work by Wong *et al.*,[25] 11 136 IR transitions were collected, yielding a spectroscopic network of 4106 energy levels. To retrieve the energy levels of $A^2\Sigma^+$, $B^2\Pi$, and $C^2\Pi$ states, we extracted further 9861 transitions (including 3393 γ, 5103 β, 1004 δ, and 361 Heath transitions) from the data sources listed in Table II. The vibronic structure of the spectroscopic network is illustrated in Fig. 5.

Although there are studies that report measured transition frequencies for the four band systems of interest, only the most reliable datasets were included in our MARVEL analysis. For example, Lagerqvist and Miescher published the line position data of 20 bands of the β and δ systems [β(5, 0) to β(19, 0) and δ(0, 0) to δ(4, 0), respectively] in 1958 (58LaMi[26]), but half of them were replaced by more accurate line lists measured by Yoshino *et al.* around 2000 (94MuYoEs,[56] 98YoEsPa,[35] 00ImYoEs,[57] 02ChLoLe,[58] 02RuYoTh,[59] and 06YoThMu[28]).

TABLE II. Data sources used in the final MARVEL analysis.

Source	Band	J''_{min}	J''_{max}	Uncertainty (cm^{-1})	Trans.[a] (A)	(V)
97DaDoKe[27]	γ(0, 0)	0.5	41.5	0.04–0.15	304	277
97DaDoKe	γ(0, 1)	0.5	40.5	0.04–0.15	277	245
97DaDoKe	γ(0, 2)	1.5	39.5	0.04–0.15	339	317
97DaDoKe	γ(0, 3)	1.5	38.5	0.04–0.1	289	279
97DaDoKe	γ(0, 4)	1.5	42.5	0.04–0.1	294	283
97DaDoKe	γ(0, 5)	1.5	37.5	0.04–0.1	266	249
97DaDoKe	γ(0, 6)	1.5	31.5	0.04–0.15	158	142
97DaDoKe	γ(1, 0)	0.5	30.5	0.04–0.15	302	275
97DaDoKe	γ(1, 4)	0.5	41.5	0.04–0.15	295	277
97DaDoKe	γ(1, 5)	1.5	39.5	0.04–0.15	142	135
97DaDoKe	γ(2, 6)	1.5	40.5	0.04–0.15	277	246
97DaDoKe	γ(2, 7)	2.5	41.5	0.04–0.15	160	155
02ChLoLe[58]	γ(3, 0)	0.5	24.5	0.03–0.05	227	205
97DaDoKe	γ(3, 4)	4.5	32.5	0.04–0.2	63	56
27JeBaMu[41]	β(0, 4)	0.5	24.5	0.2	122	52
27JeBaMu	β(0, 5)	0.5	24.5	0.2	152	143
27JeBaMu	β(0, 6)	0.5	24.5	0.2	126	124
27JeBaMu	β(0, 7)	0.5	29.5	0.2	202	200
27JeBaMu	β(0, 8)	0.5	31.5	0.2	206	204
27JeBaMu	β(0, 9)	0.5	31.5	0.2	192	188
27JeBaMu	β(0, 10)	0.5	31.5	0.2	208	202
27JeBaMu	β(0, 11)	0.5	31.5	0.2	184	180
27JeBaMu	β(0, 12)	0.5	22.5	0.2	138	138
27JeBaMu	β(1, 6)	0.5	19.5	0.2	123	119
27JeBaMu	β(1, 11)	0.5	24.5	0.2	148	142
27JeBaMu	β(1, 13)	0.5	23.5	0.2	154	150
27JeBaMu	β(2, 9)	0.5	22.5	0.2	138	130
27JeBaMu	β(2, 13)	0.5	21.5	0.2	128	128
27JeBaMu	β(2, 14)	0.5	21.5	0.2	144	139
27JeBaMu	β(2, 15)	0.5	24.5	0.2	102	99
92FaCo[60]	β(3, 0)	0.5	31.5	0.05–0.1	432	426
96DrWo[61]	β(4, 0)	0.5	8.5	0.003–0.004	66	66
96DrWo	β(5, 0)	0.5	7.5	0.003–0.005	52	52
58LaMi[26]	β(5, 0)	8.5	14.5	0.2	36	36
02ChLoLe	β(6, 0)	0.5	17.5	0.03–0.1	138	135
94MuYoEs[56]	β(7, 0)	0.5	7.5	0.03–0.1	76	60
58LaMi	β(7, 0)	6.5	16.5	0.2–0.25	70	64
58LaMi	β(8, 0)	0.5	16.5	0.2	124	120
98YoEsPa[35]	β(9, 0)	0.5	23.5	0.02–0.03	188	178
06YoThMu[28]	β(10, 0)	0.5	12.5	0.03–0.15	218	193
02RuYoTh[59]	β(11, 0)	0.5	17.5	0.03–0.08	134	125
06YoThMu	β(12, 0)	0.5	20.5	0.03–0.15	188	173
58LaMi	β(13, 0)	11.5	18.5	0.2	97	97
06YoThMu	β(14, 0)	0.5	20.5	0.03–0.08	196	153
58LaMi	β(15, 0)	0.5	17.5	0.2–0.5	239	215
58LaMi	β(16, 0)	0.5	14.5	0.2–0.3	138	133
58LaMi	β(17, 0)	0.5	11.5	0.2–0.5	42	42
58LaMi	β(18, 0)	0.5	12.5	0.2–0.5	120	108
58LaMi	β(19, 0)	0.5	12.5	0.2–0.5	82	80
94MuYoEs	δ(0, 0)	0.5	20.5	0.03–0.1	225	217
00ImYoEs[57]	δ(1, 0)	0.5	18.5	0.03–0.1	261	205
06YoThMu	δ(2, 0)	0.5	21.5	0.03–0.15	250	210
06YoThMu	δ(3, 0)	0.5	18.5	0.03–0.08	138	109
58LaMi	δ(4, 0)	0.5	11.5	0.2–0.6	130	120
82AmVe[62]	Heath(0, 0)	0.5	11.5	0.01	361	360

[a]Number of measured (A) and validated (V) Transitions.

The spectroscopic network in MARVEL[63] is established in accordance with the upper and lower quantum numbers of the transitions. We used five quantum numbers, as shown in Table III, to uniquely label the rovibronic energy levels. The quantum numbers of some transitions were improperly assigned. New assignments plus some other comments on the sources are given below:

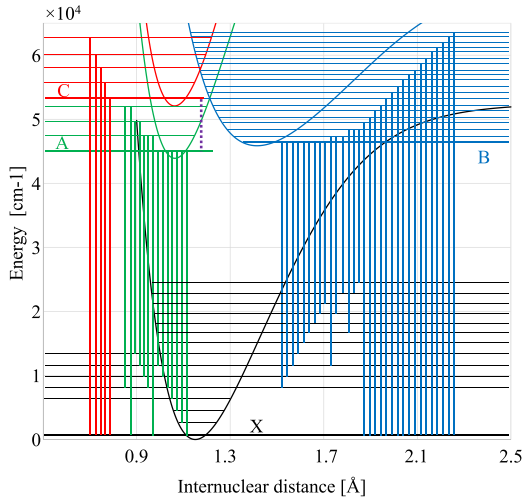

FIG. 5. Vibronic structure of the MARVEL analysis. The vertical solid lines in green, blue, and red illustrate the bands of γ, β, and δ systems, respectively. The vertical dashed line in purple represents the Heath (0, 0) band.

- In some cases (e.g., for the $A^2\Sigma^+$ state, the Q_{21} branch is indeed a copy of the R_{11} branch as listed in 97DaDoKe[27]), duplicate transition is provided in source data. In 27JeBaMu,[41] 58LaMi,[26] etc., Λ − *doubling* fine structures of many transitions are not resolved; therefore, we simply created two transitions differing in *e/f* parity with the same frequency in the MARVEL dataset.
- The uncertainties of the transitions of 27JeBaMu[41] and 58LaMi[26] were given by the combination difference test, referring to the energies of the $X^2\Pi$ state.[25]
- The uncertainties of most validated transitions are close to the lower bounds listed in Table II (see the supplementary material).
- The transitions of γ(3, 0), β(6, 0), and β(11, 0) bands extracted from 02ChLoLe,[58] 02ChLoLe,[58] and 02RuYoTh[59] were increased by +0.083 cm^{-1}, +0.083 cm^{-1}, and +0.067 cm^{-1}, respectively, as suggested in 05ThRuYo.[64] The uncertainties of these transitions should be 0.1 cm^{-1} because the absolute frequencies were not calibrated.[64] However, we used relative accuracy, i.e., 0.03 cm^{-1}, as the lower bound of uncertainty to constrain the MARVEL analysis. The uncertainties should be adjusted to 0.1 cm^{-1} if data of higher accuracy are included in the future.

TABLE III. Quantum numbers used in the MARVEL analysis.

Quan. No.	Meaning
State	Electronic state label, e.g., X stands for $X^2\Pi$
J	Total angular momentum
Parity	+ Or −
v	Vibration quantum number
Ω	Projection of the total angular momentum on the internuclear axis

- In the β(10, 0) band of 06YoThMu,[28] $R_{11}(3.5)$ and $P_{11}(3.5)$ were exchanged; the R_{21} and P_{21} branches were exchanged.
- In the δ(0, 0) band of 94MuYoEs,[56] $P_{12}(15.5)_e$ and $P_{12}(16.5)_f$ should be $P_{22}(15.5)_e$ and $P_{22}(16.5)_e$, respectively.
- In the δ(1, 0) band of 00ImYoEs,[57] the frequencies of $R_{12}(15.5)_e$ and $R_{12}(15.5)_f$ should be exchanged; the frequencies of $P_{11}(5.5)$ and $P_{11}(16.5)_f$ should be 54 668.636 cm^{-1}.
- In the δ(2, 0) band of 06YoThMu,[28] the frequencies of $Q_{22}(5.5)_e$ and $Q_{22}(6.5)_e$ should be 56 967.72 cm^{-1} and 56 966.61 cm^{-1}, respectively.
- The transitions, $R_{22}(0.5)_{ff}$, $Q_{22}(0.5)_{fe}$, $R_{12}(0.5)_{ee}$ of 97DaDoKe,[27] and $R_{22}(0.5)$ of 02ChLoLe,[58] are related to unknown lower states (J = 0.5 and Ω = 1.5). Those transitions were not validated.

The most serious issue we encountered concerned the 2020 measurements of Ventura and Fellows (20VeFe[65]) who published a new line list for the γ system containing 6436 transitions. The transitions of 20VeFe disagree with those measured by Danielak *et al.* (97DaDoKe).[27] MARVEL and combination difference analysis indicate that their dataset is self-consistent within the claimed accuracy, i.e., 0.005 cm^{-1}–0.06 cm^{-1}. However, it is inconsistent with the ground state MARVEL energies of Wong *et al.*[25] The combination difference test shows that the standard deviations of most energy levels calculated by the dataset are greater than 0.1 cm^{-1}.

In contrast, the line list of 97DaDoKe[27] is consistent with others. The measurements of 20VeFe differ from those of 97DaDoKeby up to 0.7 cm^{-1}, as acknowledged by 20VeFe. The transitions in the γ(3, 4) band measured by 97DaDoKe are consistent with the transitions in the γ(3, 0) band measured by Cheung *et al.* (02ChLoLe).[58] Furthermore, the use of Heath band potential provides a closed loop or cycle by following γ(0, 0)–Heath(0, 0)–δ(0, 0). The measurements of 97DaDoKe gave consistency in this cycle, within the stated uncertainties of the various measurements, but 20VeFe did not. Analyzing the ground state data and 20VeFe individually, we observed an average 0.43 cm^{-1} shift for the lower three vibrational levels of the $A^2\Sigma^+$ state; these energy differences are plotted in Fig. 6. We were therefore forced to conclude that the measurements of 20VeFe are not consistent with the other measurements, and these data were excluded from our MARVEL analysis.

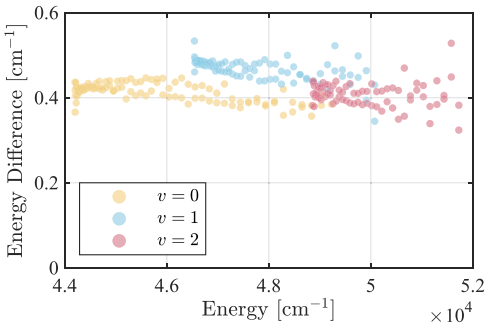

FIG. 6. The differences between the $A^2\Sigma^+$ state MARVEL energies corresponding to 20VeFe and those obtained from the sources of Table II. The average energy shift is 0.43 cm^{-1}.

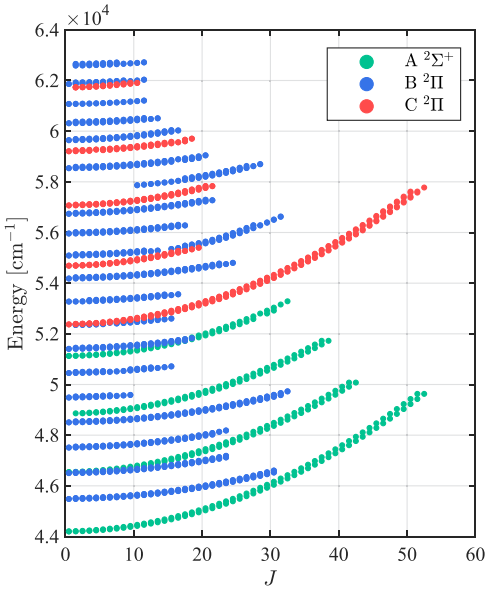

FIG. 7. $A^2\Sigma^+$, $B^2\Pi$, and $C^2\Pi$ state energy levels generated by MARVEL analysis.

The 20 293 validated transitions (including 3141 γ, 4795 β, 861 δ, and 360 Heath transitions) yielded 327, 1400, and 466 energy levels of the $A^2\Sigma^+$, $B^2\Pi$, and $C^2\Pi$ states, respectively. These levels are plotted as a function of total angular momentum J in Fig. 7. The MARVEL transitions (input) file and energies (output) file are given as part of the supplementary material.

Sulakshina and Borkov compared the ground state energies calculated by their RITZ code[66] with our previous MARVEL result.[25] The MARVEL analysis here updates the energy values of the $X^2\Pi$ state by including new rovibronic transitions; as shown in Fig. 8, the energy gaps between the results of the MARVEL and RITZ analysis are narrowed as a result of this. This is especially true for high J levels belonging to the $\Omega = \frac{3}{2}$ series [see Fig. 8(b) of Ref. 66]. The majority of levels agree within the uncertainty of their determination.

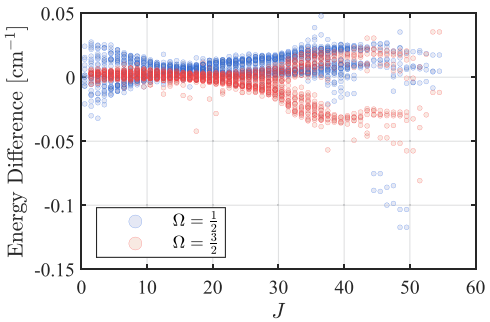

FIG. 8. Energy difference of the $X^2\Pi$ state between the MARVEL result in this paper and the RITZ result in the work of Sulakshina and Borkov.[66]

IV. REFINEMENT OF CURVES FOR $^{14}N^{16}O$

A. Calculation setup

The PECs of $A^2\Sigma^+$, $B^2\Pi$, and $C^2\Pi$, as well as other coupling curves, were refined based on the empirical energy levels yielded by the MARVEL analysis in Sec. III; the PEC for the $X^2\Pi$ state was left unchanged from that of Wong *et al.*[25] The refinement was executed in Duo, which is a general variational nuclear-motion program for calculating the spectra of diatomic molecules.[67]

Duo solves the diatomic molecular Schrödinger equation in two steps. First, the rotation-free radial equation of each electronic state is solved to get the vibrational energy levels, E_v, and wavefunctions, $\psi_v(r)$,

$$-\frac{\hbar^2}{2\mu}\frac{\mathrm{d}^2}{\mathrm{d}r^2}\psi_v(r) + V_{\text{state}}(r)\psi_v(r) = E_v\psi_v(r), \tag{1}$$

where μ is the reduced mass of the molecule and $V_{\text{state}}(r)$ is the potential energy curve. This step creates vibrational basis functions, $|\text{state}, v\rangle$. Second, the fully coupled, rovibronic Hamiltonian is diagonalized under the Hund's case (a) rovibronic basis set defined by

$$|\text{state}, J, \Omega, \Lambda, S, \Sigma, v\rangle = |\text{state}, \Lambda, S, \Sigma\rangle|J, \Omega, M\rangle|\text{state}, v\rangle, \tag{2}$$

where $|\text{state}, \Lambda, S, \Sigma\rangle$ and $|J, \Omega, M\rangle$ represent the electronic and rotational basis functions, respectively.[68] The quantum number M is the projection of the total angular momentum along the laboratory Z-axis.

Users are asked to set up some super-parameters to get the correct solution. The calculation setup for the refinement of $^{14}N^{16}O$ is summarized below. More details can be found in the Duo input file, which is given as the supplementary material and includes the PEC parameters.

- Equation (1) was solved by the Sinc-DVR (discrete variable representation) method.[69]
- The calculation range was from 0.6 Å to 4.0 Å.
- The number of grids points was 701, uniformly spaced.
- The numbers of vibrational basis sets for $X^2\Pi$, $A^2\Sigma^+$, $B^2\Pi$, and $C^2\Pi$ were 60, 15, 30, and 10, respectively.
- The maximum total angular momentum considered here was $52\frac{1}{2}$.
- The upper bound of the total energy was 65 000 cm^{-1}.

B. Refinement results of the $A^2\Sigma^+$ state

The PEC of the $A^2\Sigma^+$ state is represented by a fourth-order Extended Morse Oscillator (EMO) function.[70] The EMO is defined as a function of internuclear distance, r,

$$V(r) = T_e + (D_e - T_e)[1 - \exp(-\beta_{\text{EMO}}(r)(r - r_e))]^2, \tag{3}$$

where the distance-dependent coefficient β_{EMO} is expressed as

$$\beta_{\text{EMO}}(r) = \sum_{i=0}^{N} b_i y_p^{\text{eq}}(r)^i. \tag{4}$$

The reduced variable $y_p^{\mathrm{eq}}(r)$ has the formula

$$y_p^{\mathrm{eq}}(r) = \frac{r^p - (r_e)^p}{r^p + (r_e)^p}, \tag{5}$$

where p controls the shape of $y_p^{\mathrm{eq}}(r)$. The programmed EMO function in Duo is not exactly the same as defined by Eq. (3). A reference point R_{ref} (usually the equilibrium internuclear distance) divides the curve into left and right parts. The numbers of terms N, as well as p, for the left and right parts can be assigned different values, i.e., N_{L}, N_{R}, p_{L}, and p_{R}. The unknown dissociation energy of the state is regarded as a dummy parameter in the refinement. The initial guess of D_e was given by a pure Morse function and the value was fine-tuned in each iteration. The optimal parameters of the EMO function is listed in Table IV. The *ab initio* and refined PECs of the $A^2\Sigma^+$ state are compared in panel (a) of Fig. 9.

In addition, our model of the $A^2\Sigma^+$ state contains a spin–rotational term. In Duo, the nonzero diagonal and off-diagonal matrix elements of the spin–rotational operator $\hat{H}_{\mathrm{SR}}$[68] are given by

$$\langle \Lambda, S, \Sigma | \hat{H}_{\mathrm{SR}} | \Lambda, S, \Sigma \rangle = \frac{\hbar^2}{2\,\mu r^2} \gamma^{\mathrm{SR}}(r) \left[\Sigma^2 - S(S+1) \right], \tag{6}$$

$$\langle \Lambda, S, \Sigma | \hat{H}_{\mathrm{SR}} | \Lambda, S, \Sigma \pm 1 \rangle = \frac{\hbar^2}{4\,\mu r^2} \gamma^{\mathrm{SR}}(r) \sqrt{S(S+1) - \Sigma(\Sigma \pm 1)} \times \sqrt{J(J+1) - \Omega(\Omega \pm 1)}. \tag{7}$$

The dimensionless spin–rotational coefficient $\gamma^{\mathrm{SR}}(r)$ of the $A^2\Sigma^+$ state was modeled as a constant whose value is

$$\gamma_{\mathrm{A}}^{\mathrm{SR}}(r) = -2.080\,430\,044\,787\,81 \times 10^{-3}. \tag{8}$$

C. Refinement results of the $B^2\Pi$–$C^2\Pi$ coupled states

1. Deperturbation of the $B^2\Pi$–$C^2\Pi$ interaction

For this work, we only consider coupling between two electronic states. The interaction between two electronic states belonging to the same irreducible representation of the molecular point group directly depends on the avoided crossing of their diabatic PECs. Thus, it is possible to model the coupled states by introducing two adiabatic potentials.[71] This could be accomplished by diagonalizing the matrix,

$$\begin{pmatrix} V_1(r) & W(r) \\ W(r) & V_2(r) \end{pmatrix}, \tag{9}$$

where $V_1(r)$ and $V_2(r)$ are two diabatic potentials and $W(r)$ is the coupling curves. The adiabatic PECs, i.e., the eigenvalues of the matrix, are

$$V_{\mathrm{low}}(r) = \frac{V_1(r) + V_2(r)}{2} - \frac{\sqrt{[V_1(r) - V_2(r)]^2 + 4W^2(r)}}{2}, \tag{10}$$

$$V_{\mathrm{upp}}(r) = \frac{V_1(r) + V_2(r)}{2} + \frac{\sqrt{[V_1(r) - V_2(r)]^2 + 4W^2(r)}}{2}. \tag{11}$$

EMO potential functions are used to model $V_1(r)$ and $V_2(r)$ in Eqs. (10) and (11), while $W(r)$ is given by

$$W(r) = \frac{\sum_{i \geq 0} w_i (r - r_0)^i}{\cosh(b(r - r_0))}. \tag{12}$$

The function rapidly decreases to W_0 when r moves away from r_0.

The coupled PECs of $X\,^1\Sigma_g^+$ and $B'\,^1\Sigma_g^+$ states of C_2 were represented by adiabatic potential in our previous work,[72] producing the accurate line list. Nevertheless, this method is not optimal for

TABLE IV. The optimized EMO parameters of the PECs of $A^2\Sigma^+$, $B^2\Pi$, and $C^2\Pi$ states and the spin–orbit (SO) coupling within the $B^2\Pi$ state. The parameters are given electronically in the Duo input, which is given in the supplementary material.

Parameter	$A^2\Sigma^+$	$B^2\Pi$	$C^2\Pi$	$\langle B^2\Pi \vert \hat{H}_{\mathrm{SO}} \vert B^2\Pi \rangle$
T_e (cm^{-1})	4.390 299 277 309 43 × 10^4	4.586 704 506 760 95 × 10^4	5.208 197 358 398 84 × 10^4	8.497 424 004 318 92 × 10
r_e, r_{ref} (Å)	1.063 666 008 368 62	1.416 639 772 450 69	1.063 704 708 372 54	1.1
D_e (cm^{-1})	1.292 051 390 303 94 × 10^5	7.162 7 × 10^4	1.271 773 188 884 36 × 10^5	5.774 077 920 425 91 × 10^1
P	4	4	4	4
N_{l}	2	4	2	4
N_{r}	4	8	4	4
b_0 (Å^{-1})	2.704 913 981 796 78 × 10	2.150 144 139 754 52 × 10	2.863 985 603 255 24 × 10	2.015 987 559 388 54 × 10
b_1 (Å^{-1})	2.073 903 440 604 48 × 10^{-2}	9.835 900 997 934 13 × 10^{-2}	5.525 275 335 431 32 × 10^{-1}	0
b_2 (Å^{-1})	8.149 010 097 829 77 × 10^{-2}	4.118 983 730 047 04 × 10^{-1}	3.452 639 965 214 17 × 10	−3.768 976 845 482 42 × 10
b_3 (Å^{-1})	−9.539 702 892 896 83 × 10^{-1}	0	−3.788 700 193 112 05 × 10^1	0
b_4 (Å^{-1})	2.050 677 385 076 37 × 10	−4.436 396 750 585 21 × 10^{-1}	8.286 317 439 495 08 × 10^1	6.672 511 527 886 65 × 10
b_5 (Å^{-1})		1.215 719 272 327 52 × 10^1		
b_6 (Å^{-1})		−1.784 795 357 577 77 × 10^1		
b_7 (Å^{-1})		3.127 784 544 525 73E+00		
b_8 (Å^{-1})		5.403 077 729 588 00E+00		

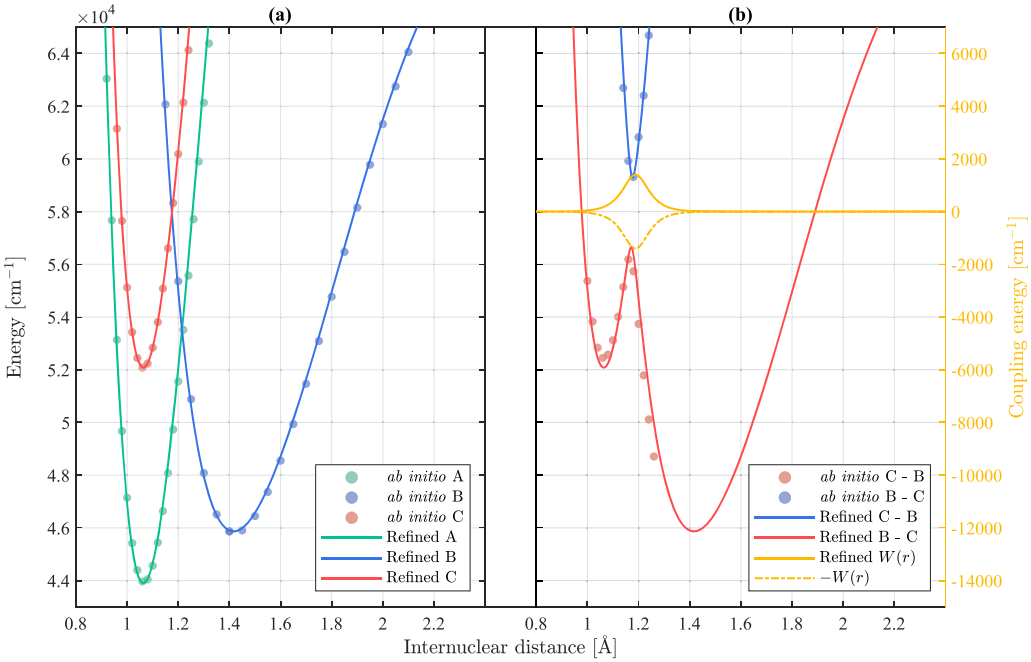

FIG. 9. The *ab initio* and refined PECs of the $A^2\Sigma^+$, $B^2\Pi$, and $C^2\Pi$ states as well as the refined B– C interaction term $W(r)$. (a) Diabatic and (b) adiabatic representations. The refined potential curves in panel (b) is calculated using Eqs. (10) and (11). The *ab initio* curves are shifted using empirical T_e values.

NO where the avoided crossing between the B and C states is very sharp. Thus, for example, the adiabatic B–X and C–X transition dipole moment curves (TDMCs) change dramatically around the crossing point, making them hard to use in any reliable calculation of transition intensities, and a slight shift of the crossing point, r_0, during refinement may significantly change the intensities of nearby lines. We therefore adopt the following procedure for the generating line lists involving these coupled electronic states:

1. Solve the radial equations set up with diabatic PECs of different electronic states to get vibrational basis.
2. Construct the rovibronic Hamiltonian matrix with all necessary elements, including the electronic interaction terms.
3. Diagonalize the matrix under rovibronic basis set to get the rovibronic energy levels and the corresponding wavefunctions.
4. Refine the diabatic PECs, electronic interaction terms, and other coupling curves by fitting the energies to observed energy levels.
5. Calculate the Einstein A coefficient with the diabatic TDMCs, and let the wavefunctions determine the weights of TDMCs for each rovibronic state at different geometries.

The method not only rescues us from the dilemma of constructing adiabatic TDMCs but also improves the flexibility of our program. For instance, it is convenient to model the $B^2\Pi$–$C^2\Pi$–$L^2\Pi$ coupled states of NO by adding new definitions of the potential of $L^2\Pi$ and coupled term between $C^2\Pi$ and $L^2\Pi$ in the input file of Duo, without changing its code.

2. Refined curves

The diabatic PECs of $B^2\Pi$ and $C^2\Pi$ states were modeled using EMO functions whose optimal parameters are listed in Table IV. The *ab initio* and refined PECs of $B^2\Pi$ and $C^2\Pi$ states are compared in panel (a) Fig. 9. The optimal parameters of the function are listed in Table V. Although not used in this work, the adiabatic curves were calculated as defined by Eqs. (10) and (11). They are compared with the *ab initio* adiabatic PECs in panel (b) of Fig. 9. The dissociation energy of the $C^2\Pi$ state is also a dummy parameter. The refined PECs of $A^2\Sigma^+$ and $C^2\Pi$ states are physically meaningless outside our calculation range (i.e., when energy is greater than 65 000 cm^{-1}).

The spin–orbit coupling curve (SOC) of the $B^2\Pi$ state was also fitted to an EMO function whose optimal parameters are listed in the last column of Table IV. Figure 10 compares the *ab initio* and refined SOCs. The diagonal spin-orbital term of the $C^2\Pi$ state and the off-diagonal term between $B^2\Pi$ and $C^2\Pi$ were determined empirically

TABLE V. Optimized Lorentz parameters for the B–C interaction curve.

Parameter	Value
b ($Å^{-1}$)	$2.217\,076\,306\,467\,40 \times 10^1$
r_0 (Å)	1.188 085 737 226 98
w_0 (cm^{-1})	$1.401\,731\,787\,542\,00 \times 10^3$

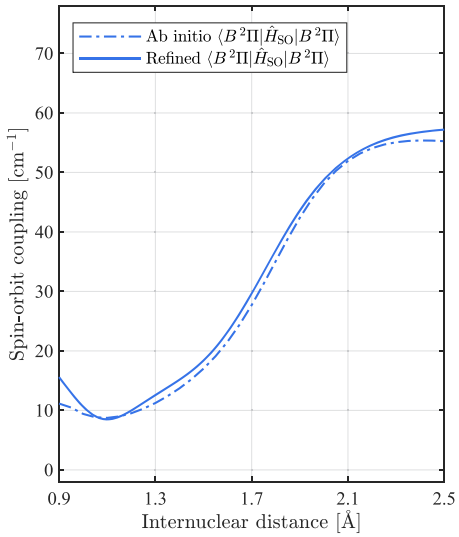

FIG. 10. The spin–orbit coupling curves of $B^2\Pi$ states.

TABLE VI. Optimized values of the spin–orbit (SO) and spin–rotation (SR) coupling terms.

Term	Value
$\langle C\,^2\Pi|\hat{H}_{SO}|C\,^2\Pi\rangle$ [cm^{-1}]	1.817 667 722 287 87 × 10
$\langle C\,^2\Pi|\hat{H}_{SO}|B\,^2\Pi\rangle$ [cm^{-1}]	2.282 063 757 469 38 × 10
γ_C^{SR}	2.705 930 617 891 97 × 10^{-3}

by fitting to constants. The spin–rotational coefficient of the $C^2\Pi$ state was also model on a constant. The values of these terms are listed in Table VI.

The Λ − *doubling* fine structures of β and δ system bands were observed in most of the work listed in Table II. Duo calculates the Λ − *doubling* matrix elements, i.e., $\langle \Lambda'\Sigma'J'\Omega'|\hat{H}_{LD}|\Lambda''\Sigma''J''\Omega''\rangle$, according to the terms given by Brown and Merer,[73]

$$\langle \mp 1, \Sigma \pm 2, J, \Omega|\hat{H}_{LD}|\pm 1, \Sigma, J, \Omega\rangle = \frac{1}{2}(o_v + p_v + q_v) \times \sqrt{[S(S+1) - \Sigma(\Sigma \pm 1)][S(S+1) - (\Sigma \pm 1)(\Sigma \pm 2)]}, \quad (13)$$

$$\langle \mp 1, \Sigma \pm 1, J, \Omega \mp 1|\hat{H}_{LD}|\pm 1, \Sigma, J, \Omega\rangle = -\frac{1}{2}(p_v + 2q_v) \times \sqrt{[S(S+1) - \Sigma(\Sigma \pm 1)][J(J+1) - \Omega(\Omega \mp 1)]}, \quad (14)$$

$$\langle \mp 1, \Sigma, J, \Omega \mp 2|\hat{H}_{LD}|\pm 1, \Sigma, J, \Omega\rangle = \frac{1}{2}q_v \times \sqrt{[J(J+1) - \Omega(\Omega \mp 1)][J(J+1) - (\Omega \mp 1)(\Omega \mp 2)]}. \quad (15)$$

For $B^2\Pi$ and $C^2\Pi$, $\Sigma = \pm 1/2$. Therefore, the matrix elements described in Eq. (13) are zero, and only the coefficient curves of Eqs. (14) and (15) were fitted to polynomials, i.e.,

$$P(r) = a_0 + \sum_{i \geq 0} a_i (r - r_0)^i. \quad (16)$$

The optimized parameters of the Λ − *doubling* terms are listed in Table VII.

3. Fitting residues of the rovibronic energy levels

The fitting residues of the $A^2\Sigma^+$ state are shown in panel (a) of Fig. 11. The high-J energies of $v = 3$ vibrational levels are mainly determined by blended lines of 97DaDoKe.NO.[27] The fitting residues of the $B^2\Pi$ and $C^2\Pi$ states are shown in panel (b) of Fig. 11, where the cold colors represent the $B^2\Pi$ state and the warm ones represent the $C^2\Pi$ state. The F_1 (i.e., $\Omega = \frac{1}{2}$) and F_2 (i.e., $\Omega = \frac{3}{2}$) levels are also distinguishable. The residue distributions indicate J-dependent systematic error of our model, which may result from some off-diagonal couplings, e.g., the coupling between $C^2\Pi$ and $D^2\Sigma^+$ states.[62]

The residues of all rovibronic energy levels are plotted against their corresponding uncertainties in Fig. 12. The root-mean-square and average value of uncertainties and residues are compared in Table VIII.

The accuracy of our model is definitely higher than those of Lagerqvist and Miescher[26] or Gallusser and Dressler.[37] On the one hand, the most recent measurements (e.g., the works of Yoshino *et al.*[28]) and spectroscopic analysis techniques (MARVEL[63]) helped us reconstruct reliable spectroscopic network and energy levels. On the other hand, our model was directly fitted to the

TABLE VII. Optimized polynomial parameters of the Λ — doubling curves of the $B^2\Pi$ and $C^2\Pi$ states.

	$B^2\Pi$		$C^2\Pi$	
Parameter	$p_v + 2q_v$	q_v	$p_v + 2q_v$	q_v
r_0 (Å)	1.416 504 703 523 37 × 10	1.416 504 703 523 37 × 10	0	1.064 436 059 412 32 × 10
a_0 (cm^{-1})	1.065 516 703 466 50 × 10^{-2}	6.453 326 916 333 86 × 10^{-5}	−3.660 394 013 643 46 × 10^{-2}	−1.612 437 381 504 96 × 10^{-2}
a_1 (cm^{-1}Å^{-1})	−2.921 142 813 629 27 × 10^{-1}	−1.189 741 089 831 74 × 10^{-2}	0	3.003 216 097 917 86 × 10^{-2}
a_2 (cm^{-1}Å^{-2})	5.095 170 164 836 91 × 10^{-1}	3.040 771 809 152 39 × 10^{-2}	0	0

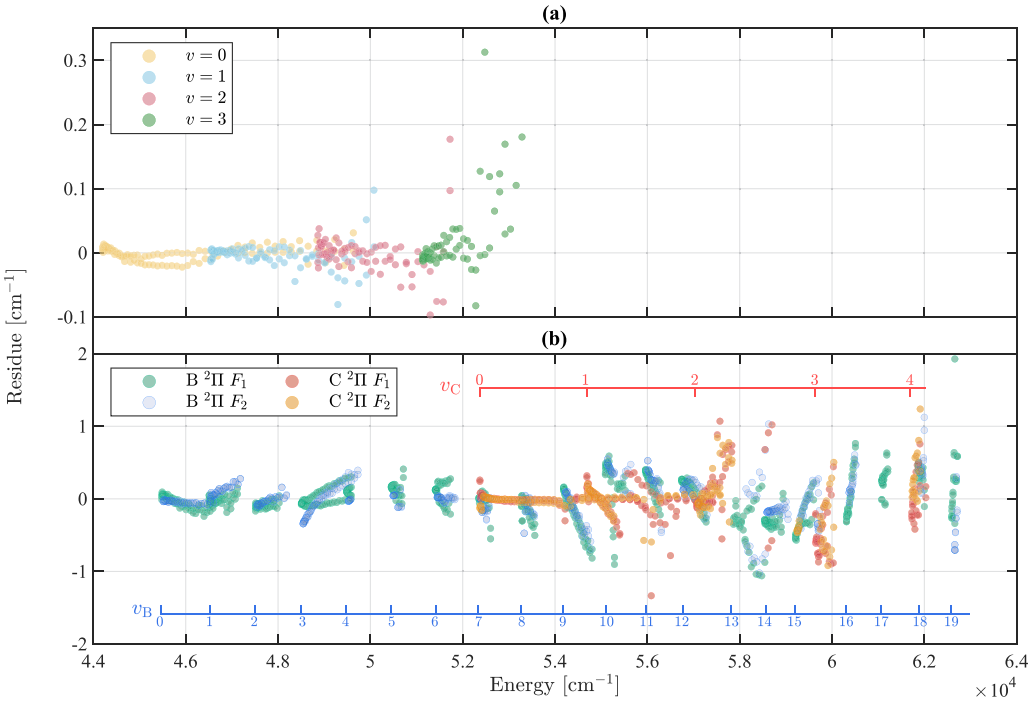

FIG. 11. Fitting residues of (a) $A^2\Sigma^+$ state and (b) $B^2\Pi$–$C^2\Pi$ coupled states.

observed rovibronic levels. The vibronic residues given by Gallusser and Dressler[37] are greater than our rovibronic residues. Unlike Gallusser and Dressler, we did not include higher electronic states, such as $L^2\Pi$ and $K^2\Pi$, in our model, which reduces its range of applicability where the state energy is greater than 63 000 cm^{-1}. However, thanks to diabatic coupling strategy of Duo, the model can easily be updated in a future study.

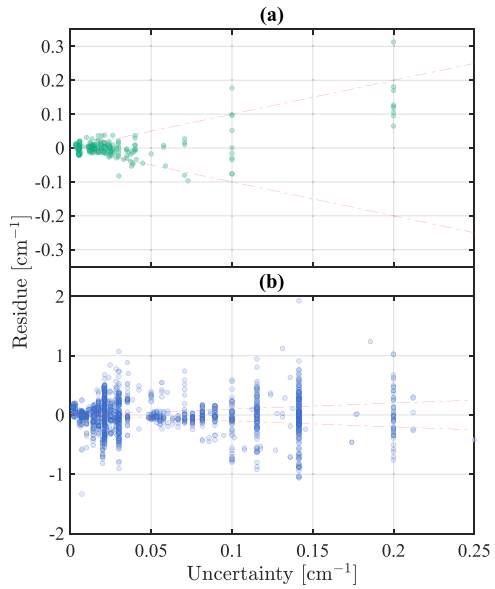

FIG. 12. Residues against uncertainties of (a) $A^2\Sigma^+$ state and (b) B–C coupled states with vibrational states given in the bars.

We note that some of the assignments to B or C electronic states differ between Duo and our MARVEL analysis. Duo uses three good quantum numbers, namely, the total angular momentum J, the total parity, and the counting number of the levels with the same values of J and parity. The other quantum numbers such as state, v, and Ω are estimated using the contribution of the basis functions to a given wavefunction. It is to be anticipated that in regions of heavily mixed wavefunctions, this may lead to differences compared to other assignment methods. The MARVEL and Duo energy levels of the B (v = 13)–C (v = 2) coupled series are plotted in Fig. 13. Table IX lists some energy levels in the output .en file of Duo. Both of them demonstrate the differences between the quantum numbers of MARVEL and Duo results.

TABLE VIII. Overall comparison of the uncertainty and residue.

All in cm^{-1}	$A^2\Sigma^+$	$B^2\Pi$-$C^2\Pi$
RMS uncertainty	0.042 84	0.079 27
RMS residue	0.033 90	0.272 17
Average uncertainty	0.024 53	0.057 53
Average absolute residue	0.015 99	0.18603

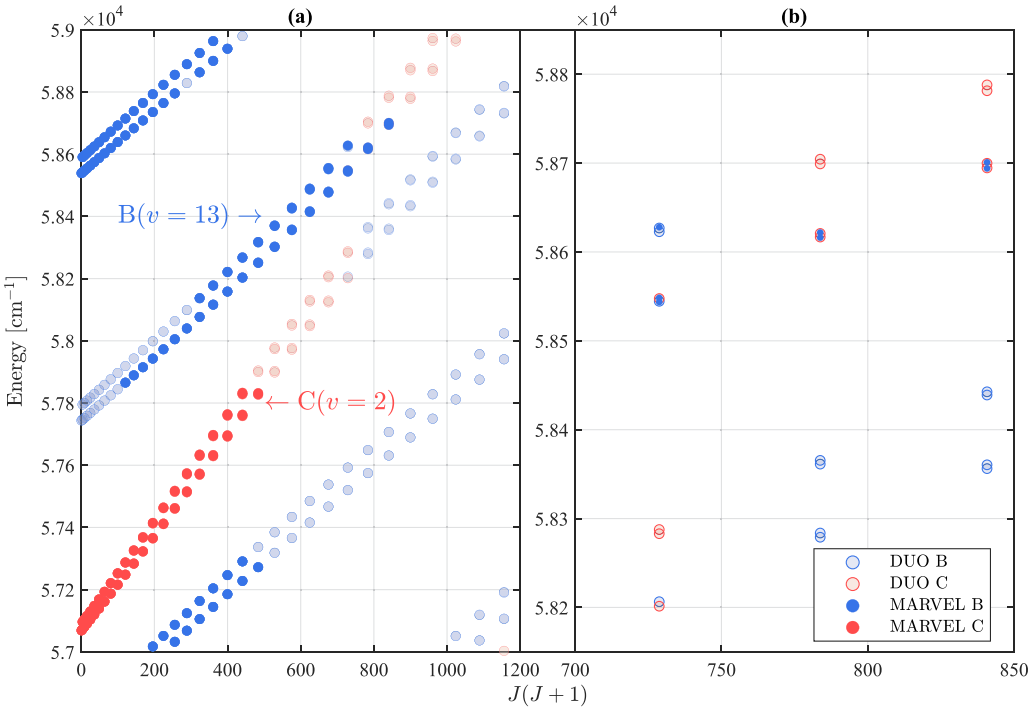

FIG. 13. Calculated and observed energy levels of the B(v = 13)–C(v = 2) coupled series. The right-hand side panel is a blow up of the avoided crossing between the states, which gives a clearer view of the Λ − doubling splitting and the difference between the quantum numbers given by MARVEL and Duo.

TABLE IX. Sample lines extracted from the output .en file of Duo.

Duo	Assigned			MARVEL	Duo			Duo					MARVEL				
N	N[a]	J	Parity	Energy	Energy	Residue	Weight	state[b]	v	Λ	Σ	Ω	state[b]	v	Λ	Σ	Ω
39	39	1.5	+	52 349.0418	52 349.0274	0.0144	9.50×10^{-5}	3	7	1	−0.5	0.5	3	7	1	−0.5	0.5
40	40	1.5	+	52 373.2372	52 373.3626	−0.1255	1.40×10^{-3}	4	0	1	0.5	1.5	3	7	1	0.5	1.5
41	41	1.5	+	52 380.1912	52 380.1101	0.0810	1.30×10^{-3}	4	0	1	−0.5	0.5	4	0	1	−0.5	0.5
42	42	1.5	+	52 392.3007	52 392.3172	−0.0165	1.30×10^{-3}	3	7	1	0.5	1.5	4	0	1	0.5	1.5
64	64	2.5	−	59 217.4976	59 217.9730	−0.4754	9.50×10^{-5}	3	15	−1	0.5	−0.5	4	3	−1	0.5	−0.5
65	65	2.5	−	59 250.3720	59 250.8248	−0.4528	9.50×10^{-5}	4	3	−1	−0.5	−1.5	4	3	−1	−0.5	−1.5
66	66	2.5	−	59 654.3005	59 654.8551	−0.5546	3.70×10^{-6}	4	3	−1	0.5	−0.5	3	15	−1	0.5	−0.5
67	67	2.5	−	59 692.2845	59 692.6292	−0.3447	4.80×10^{-6}	3	15	−1	−0.5	−1.5	3	15	−1	−0.5	−1.5

[a]The counting numbers (N) were manually assigned to match the corresponding MARVEL energy level.
[b]In these columns, "3" and "4" indicate the $B^2\Pi$ and $C^2\Pi$ states, respectively.

V. CONCLUSION

In this paper, potential energy curves and coupling for the low-lying electronic state of NO are calculated using the quantum chemistry package Molpro. The strong interaction between Rydberg and valence states makes the *ab initio* calculation challenging. We obtain both adiabatic and diabatic PECs and SOCs for the $A^2\Sigma^+$, $B^2\Pi$, and $C^2\Pi$ states. The curves were refined by fitting the rovibronic energy levels calculated by the variational nuclear motion program Duo to those reconstructed by MARVEL analysis. The rms error of the $A^2\Sigma^+$ state fitting and $B^2\Pi$–$C^2\Pi$ coupled state fitting are 0.033 90 cm^{-1} and 0.272 17 cm^{-1}, respectively, which energies were determined by our use of a MARVEL procedure and the best available measurements. The success of $B^2\Pi$–$C^2\Pi$ coupled state fitting validates our deperturbation method for treating the coupled electronic state. This work, when combined with the earlier $X^2\Pi$ study of Wong *et al.*,[25] provides a comprehensive spectroscopic model for the lowest for electronic states of NO and thus a good start point for

the generation of a NO UV line list. This line list will be presented elsewhere.

SUPPLEMENTARY MATERIAL

Three text files are provided as the supplementary material to the article: MARVEL.txt: input transitions file used with MARVEL. MARVEL.txt: energy levels file generated by MARVEL using the file MARVEL.txt. NO.model.txt: a Duo input file that fully specifies our spectroscopic model including the associated potential energy and coupling curves.

ACKNOWLEDGMENTS

We are indebted to Dr. Rafał Hakalla (University of Rzeszów) for valuable discussions. Qianwei Qu acknowledges the financial support from University College London and the China Scholarship Council. This work was supported by STFC Project Nos. ST/M001334/1 and ST/R000476/1 and ERC Advanced Investigator Project No. 883830. The authors acknowledge the use of the UCL Myriad, Grace and Kathleen High Performance Computing Facilities and associated support services in the completion of this work.

DATA AVAILABILITY

The data that support the findings of this study are available within the article and its supplementary material.

REFERENCES

[1] D. E. Canfield, A. N. Glazer, and P. G. Falkowski, Science **330**, 192 (2010).
[2] P. M. Vitousek, J. D. Aber, R. W. Howarth, G. E. Likens, P. A. Matson, D. W. Schindler, W. H. Schlesinger, and D. G. Tilman, Ecol. Appl. **7**, 737 (1997).
[3] W. L. Chameides, P. S. Kasibhatla, J. Yienger, and H. Levy, Science **264**, 74 (1994).
[4] G. E. Likens, C. T. Driscoll, and D. C. Buso, Science **272**, 244 (1996).
[5] A. Singh and M. Agrawal, J. Environ. Biol. **29**, 15 (2008).
[6] Y. Hu, S. Naito, N. Kobayashi, and M. Hasatani, Fuel **79**, 1925 (2000).
[7] Y. H. Li, G. Q. Lu, and V. Rudolph, Chem. Eng. Sci. **53**, 1 (1998).
[8] D. S. Bredt and S. H. Snyder, Neuron **8**, 3 (1992).
[9] D. S. Bredt and S. H. Snyder, Annu. Rev. Biochem. **63**, 175 (1994).
[10] M. Arasimowicz and J. Floryszak-Wieczorek, Plant Sci. **172**, 876 (2007).
[11] B. Mayer and B. Hemmens, Trends Biochem. Sci. **22**, 477 (1997).
[12] A. G. Estévez and J. Jordán, Ann. N. Y. Acad. Sci. **962**, 207 (2002).
[13] L. M. Ziurys, D. McGonagle, Y. Minh, and W. M. Irvine, Astrophys. J. **373**, 535 (1991).
[14] C. Cox, A. Saglam, J.-C. Gérard, J.-L. Bertaux, F. González-Galindo, F. Leblanc, and A. Reberac, J. Geophys. Res.: Planets **113**, E08012, https://doi.org/10.1029/2007je003037 (2008).
[15] J.-C. Gérard, C. Cox, A. Saglam, J.-L. Bertaux, E. Villard, and C. Nehmé, J. Geophys. Res. **113**, E00B03, https://doi.org/10.1029/2008je003078 (2008).
[16] J.-C. Gérard, C. Cox, L. Soret, A. Saglam, G. Piccioni, J.-L. Bertaux, and P. Drossart, J. Geophys. Res. **114**, E00B44, https://doi.org/10.1029/2009je003371 (2009).
[17] J. R. Partington, Ann. Sci. **1**, 359 (1936).
[18] J. Priestley, Philos. Trans. R. Soc. London **62**, 147 (1772).
[19] A. Deller and S. D. Hogan, J. Chem. Phys. **152**, 144305 (2020).
[20] W. G. Bessler and C. Schulz, Appl. Phys. B: Lasers Opt. **78**, 519 (2004).
[21] A. F. H. van Gessel, B. Hrycak, M. Jasiński, J. Mizeraczyk, J. J. A. M. van der Mullen, and P. J. Bruggeman, J. Phys. D: Appl. Phys. **46**, 095201 (2013).
[22] J. Tennyson and S. N. Yurchenko, Mon. Not. R. Astron. Soc. **425**, 21 (2012).
[23] J. Tennyson, S. N. Yurchenko, A. F. Al-Refaie, E. J. Barton, K. L. Chubb, P. A. Coles, S. Diamantopoulou, M. N. Gorman, C. Hill, A. Z. Lam, L. Lodi, L. K. McKemmish, Y. Na, A. Owens, O. L. Polyansky, T. Rivlin, C. Sousa-Silva, D. S. Underwood, A. Yachmenev, and E. Zak, J. Mol. Spectrosc. **327**, 73 (2016).
[24] J. Tennyson, S. N. Yurchenko, A. F. Al-Refaie, V. H. J. Clark, K. L. Chubb, E. K. Conway, A. Dewan, M. N. Gorman, C. Hill, A. E. Lynas-Gray, T. Mellor, L. K. McKemmish, A. Owens, O. L. Polyansky, M. Semenov, W. Somogyi, G. Tinetti, A. Upadhyay, I. Waldmann, Y. Wang, S. Wright, and O. P. Yurchenko, J. Quant. Spectrosc. Radiat. Transfer **255**, 107228 (2020).
[25] A. Wong, S. N. Yurchenko, P. Bernath, H. S. P. Müller, S. McConkey, and J. Tennyson, Mon. Not. R. Astron. Soc. **470**, 882 (2017).
[26] A. Lagerqvist and E. Miescher, Helv. Phys. Acta **31**, 221 (1958).
[27] J. Danielak, U. Domin, R. Ke, M. Rytel, and M. Zachwieja, J. Mol. Spectrosc. **181**, 394 (1997).
[28] K. Yoshino, A. P. Thorne, J. E. Murray, A. S.-C. Cheung, A. L. Wong, and T. Imajo, J. Chem. Phys. **124**, 054323 (2006).
[29] I. E. Gordon, L. S. Rothman, C. Hill, R. V. Kochanov, Y. Tan, P. F. Bernath, M. Birk, V. Boudon, A. Campargue, K. V. Chance, B. J. Drouin, J.-M. Flaud, R. R. Gamache, J. T. Hodges, D. Jacquemart, V. I. Perevalov, A. Perrin, K. P. Shine, M.-A. H. Smith, J. Tennyson, G. C. Toon, H. Tran, V. G. Tyuterev, A. Barbe, A. G. Császár, V. M. Devi, T. Furtenbacher, J. J. Harrison, J.-M. Hartmann, A. Jolly, T. J. Johnson, T. Karman, I. Kleiner, A. A. Kyuberis, J. Loos, O. M. Lyulin, S. T. Massie, S. N. Mikhailenko, N. Moazzen-Ahmadi, H. S. P. Müller, O. V. Naumenko, A. V. Nikitin, O. L. Polyansky, M. Rey, M. Rotger, S. W. Sharpe, K. Sung, E. Starikova, S. A. Tashkun, J. V. Auwera, G. Wagner, J. Wilzewski, P. Wcisło, S. Yu, and E. J. Zak, J. Quant. Spectrosc. Radiat. Transfer **203**, 3 (2017).
[30] N. Jacquinet-Husson, R. Armante, N. A. Scott, A. Chédin, L. Crépeau, C. Boutammine, A. Bouhdaoui, C. Crevoisier, V. Capelle, C. Boonne, N. Poulet-Crovisier, A. Barbe, D. Chris Benner, V. Boudon, L. R. Brown, J. Buldyreva, A. Campargue, L. H. Coudert, V. M. Devi, M. J. Down, B. J. Drouin, A. Fayt, C. Fittschen, J.-M. Flaud, R. R. Gamache, J. J. Harrison, C. Hill, Ø. Hodnebrog, S.-M. Hu, D. Jacquemart, A. Jolly, E. Jiménez, N. N. Lavrentieva, A.-W. Liu, L. Lodi, O. M. Lyulin, S. T. Massie, S. Mikhailenko, H. S. P. Müller, O. V. Naumenko, A. Nikitin, C. J. Nielsen, J. Orphal, V. I. Perevalov, A. Perrin, E. Polovtseva, A. Predoi-Cross, M. Rotger, A. A. Ruth, S. S. Yu, K. Sung, S. A. Tashkun, J. Tennyson, V. G. Tyuterev, J. Vander Auwera, B. A. Voronin, and A. Makie, J. Mol. Spectrosc. **327**, 31 (2016).
[31] J. Luque and D. R. Crosley, J. Quant. Spectrosc. Radiat. Transfer **53**, 189 (1995).
[32] J. Luque and D. R. Crosley, J. Chem. Phys. **111**, 7405 (1999).
[33] J. Luque and D. R. Crosley, J. Chem. Phys. **112**, 9411 (2000).
[34] J. Luque and D. R. Crosley, SRI international report MP 99 (1999).
[35] K. Yoshino, J. R. Esmond, W. H. Parkinson, A. P. Thorne, J. E. Murray, R. C. M. Learner, G. Cox, A. S.-C. Cheung, K. W.-S. Leung, K. Ito, T. Matsui, and T. Imajo, J. Chem. Phys. **109**, 1751 (1998).
[36] D. L. Albritton, A. L. Schmeltekopf, and R. N. Zare, J. Chem. Phys. **71**, 3271 (1979).
[37] R. Gallusser and K. Dressler, J. Chem. Phys. **76**, 4311 (1982).
[38] T. Furtenbacher, A. G. Császár, and J. Tennyson, J. Mol. Spectrosc. **245**, 115 (2007).
[39] R. Tóbiás, T. Furtenbacher, J. Tennyson, and A. G. Császár, Phys. Chem. Chem. Phys. **21**, 3473 (2019).
[40] H. J. Werner, P. J. Knowles, G. Knizia, F. R. Manby, M. Schütz, P. Celani, W. Győrffy, D. Kats, T. Korona, R. Lindh, A. Mitrushenkov, G. Rauhut, K. R. Shamasundar, T. B. Adler, R. D. Amos, A. Bernhardsson, A. Berning, D. L. Cooper, M. J. O. Deegan, A. J. Dobbyn, F. Eckert, E. Goll, C. Hampel, A. Hesselmann, G. Hetzer, T. Hrenar, G. Jansen, C. Köppl, Y. Liu, A. W. Lloyd, R. A. Mata, A. J. May, S. J. McNicholas, W. Meyer, M. E. Mura, A. Nicklass, D. P. O'Neill, P. Palmieri, D. Peng, K. Pflüger, R. Pitzer, M. Reiher, T. Shiozaki, H. Stoll, A. J. Stone, R. Tarroni, T. Thorsteinsson, and M. Wang, Molpro, version 2015.1, a package of *ab initio* programs, http://www.molpro.net, 2015.
[41] F. A. Jenkins, H. A. Barton, and R. S. Mulliken, Phys. Rev. **30**, 150 (1927).
[42] C. Amiot, J. Mol. Spectrosc. **94**, 150 (1982).
[43] D. C. Cartwright, M. J. Brunger, L. Campbell, B. Mojarrabi, and P. J. O. Teubner, J. Geophys. Res. **105**, 20857, https://doi.org/10.1029/1999ja000333 (2000).

[44]H.-J. Werner, P. J. Knowles, G. Knizia, F. R. Manby, and M. Schütz, Wiley Interdiscip. Rev.: Comput. Mol. Sci. **2**, 242 (2012).
[45]F. Grein and A. Kapur, J. Chem. Phys. **77**, 415 (1982).
[46]R. de Vivie and S. D. Peyerimhoff, J. Chem. Phys. **89**, 3028 (1988).
[47]H. Shi and A. L. L. East, J. Chem. Phys. **125**, 104311 (2006).
[48]J. Cheng, H. Zhang, and X. Cheng, Comput. Theor. Chem. **1114**, 165 (2017).
[49]J. Cheng, H. Zhang, X. Cheng, and X. Song, Mol. Phys. **115**, 2577 (2017).
[50]D. M. Cooper, J. Quant. Spectrosc. Radiat. Transfer **27**, 459 (1982).
[51]S. R. Langhoff, C. W. Bauschlicher, and H. Partridge, J. Chem. Phys. **89**, 4909 (1988).
[52]S. R. Langhoff, H. Partridge, C. W. Bauschlicher, and A. Komornicki, J. Chem. Phys. **94**, 6638 (1991).
[53]R. Polak and J. Fišer, Chem. Phys. Lett. **377**, 564 (2003).
[54]T. H. Dunning, J. Chem. Phys. **90**, 1007 (1989).
[55]K. P. Huber and G. Herzberg, *Molecular Spectra and Molecular Structure IV. Constants of Diatomic Molecules* (Van Nostrand Reinhold Company, New York, 1979).
[56]J. E. Murray, K. Yoshino, J. R. Esmond, W. H. Parkinson, Y. Sun, A. Dalgarno, A. P. Thorne, and G. Cox, J. Chem. Phys. **101**, 62 (1994).
[57]T. Imajo, K. Yoshino, J. R. Esmond, W. H. Parkinson, A. P. Thorne, J. E. Murray, R. C. M. Learner, G. Cox, A. S.-C. Cheung, K. Ito, and T. Matsui, J. Chem. Phys. **112**, 2251 (2000).
[58]A. S.-C. Cheung, D. H.-Y. Lo, K. W.-S. Leung, K. Yoshino, A. P. Thorne, J. E. Murray, K. Ito, T. Matsui, and T. Imajo, J. Chem. Phys. **116**, 155 (2002).
[59]J. Rufus, K. Yoshino, A. P. Thorne, J. E. Murray, T. Imajo, K. Ito, and T. Matsui, J. Chem. Phys. **117**, 10621 (2002).
[60]G. W. Faris and P. C. Cosby, J. Chem. Phys. **97**, 7073 (1992).
[61]M. Drabbels and A. M. Wodtke, Chem. Phys. Lett. **256**, 8 (1996).
[62]C. Amiot and J. Verges, Phys. Scr. **25**, 302 (1982).
[63]A. G. Császár and T. Furtenbacher, J. Mol. Spectrosc. **266**, 99 (2011).
[64]A. P. Thorne, J. Rufus, K. Yoshino, A. S.-C. Cheung, and T. Imajo, J. Chem. Phys. **122**, 179901 (2005).
[65]L. R. Ventura and C. E. Fellows, J. Quant. Spectrosc. Radiat. Transfer **246**, 106900 (2020).
[66]O. N. Sulakshina and Y. G. Borkov, J. Quant. Spectrosc. Radiat. Transfer **209**, 171 (2018).
[67]S. N. Yurchenko, L. Lodi, J. Tennyson, and A. V. Stolyarov, Comput. Phys. Commun. **202**, 262 (2016).
[68]J. Tennyson, L. Lodi, L. K. McKemmish, and S. N. Yurchenko, J. Phys. B **49**, 102001 (2016).
[69]D. T. Colbert and W. H. Miller, J. Chem. Phys. **96**, 1982 (1992).
[70]E. G. Lee, J. Y. Seto, T. Hirao, P. F. Bernath, and R. J. Le Roy, J. Mol. Spectrosc. **194**, 197 (1999).
[71]T. Karman, M. Besemer, A. van der Avoird, and G. C. Groenenboom, J. Chem. Phys. **148**, 094105 (2018).
[72]S. N. Yurchenko, I. Szabó, E. Pyatenko, and J. Tennyson, Mon. Not. R. Astron. Soc. **480**, 3397 (2018).
[73]J. M. Brown and A. J. Merer, J. Mol. Spectrosc. **74**, 488 (1979).